ACS APPLIED MATERIALS & INTERFACES

www.acsami.org

Research Article

Fine-Tuning of Pt Dispersion on Al_2O_3 and Understanding the Nature of Active Pt Sites for Efficient CO and NH_3 Oxidation Reactions

Wei Tan, Shaohua Xie, Xing Zhang, Kailong Ye, Murtadha Almousawi, Daekun Kim, Haowei Yu, Yandi Cai, Hanchen Xi, Lu Ma, Steven N. Ehrlich, Fei Gao, Lin Dong, and Fudong Liu*

Cite This: *ACS Appl. Mater. Interfaces* 2024, 16, 454−466

Read Online

ACCESS | Metrics & More | Article Recommendations | Supporting Information

ABSTRACT: Fine-tuning the dispersion of active metal species on widely used supports is a research hotspot in the catalysis community, which is vital for achieving a balance between the atomic utilization efficiency and the intrinsic activity of active sites. In this work, using bayerite $Al(OH)_3$ as support directly or after precalcination at 200 or 550 °C, Pt/Al_2O_3 catalysts with distinct Pt dispersions from single atoms to clusters (*ca.* 2 nm) were prepared and evaluated for CO and NH_3 removal. Richer surface hydroxyl groups on $AlO_x(OH)_y$ support were proved to better facilitate the dispersion of Pt. However, Pt/Al_2O_3 with relatively lower Pt dispersion could exhibit better activity in CO/NH_3 oxidation reactions. Further reaction mechanism study revealed that the Pt sites on Pt/Al_2O_3 with lower Pt dispersion could be activated to Pt^0 species much easier under the CO oxidation condition, on which a higher CO adsorption capacity and more efficient O_2 activation were achieved simultaneously. Compared to Pt single atoms, PtO_x clusters could also better activate NH_3 into $-NH_2$ and $-HNO$ species. The higher CO adsorption capacity and the more efficient NH_3/O_2 activation ability on Pt/Al_2O_3 with relatively lower Pt dispersion well explained its higher CO/NH_3 oxidation activity. This study emphasizes the importance of avoiding a singular pursuit of single-atom catalyst synthesis and instead focusing on achieving the most effective Pt species on Al_2O_3 support for targeted reactions. This approach avoids unnecessary limitations and enables a more practical and efficient strategy for Pt catalyst fabrication in emission control applications.

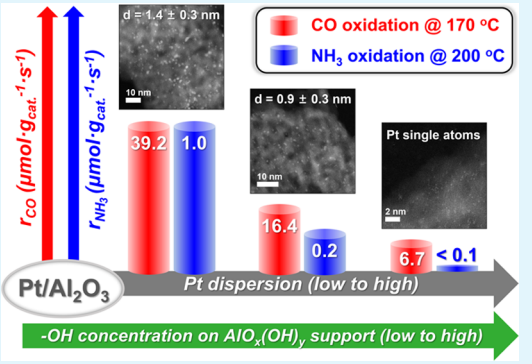

KEYWORDS: *Pt dispersion, surface hydroxyl groups, NH_3 oxidation, CO oxidation, surface reduction*

1. INTRODUCTION

A remarkable increase in vehicle ownership over the last few decades has undoubtedly enhanced people's lives. Nonetheless, the exhaust gases emitted by engines have resulted in significant harm to the environment and human health.[1,2] As a response to the escalating demand for strict emission standards, researchers have extensively studied exhaust after-treatment systems equipped with robust catalysts.[3,4] Moreover, the continuous rise in the price of platinum group metals (PGMs), which are widely used as main active components in emission control catalysts, has also prompted academia and industry to investigate the finer control of PGM dispersion on different supports, thus improving the atomic utilization efficiency of PGMs and enhancing the intrinsic activity of catalytic sites.[5]

Alumina-supported platinum (Pt/Al_2O_3) is one of the most widely used heterogeneous catalysts for the catalytic oxidation of various air pollutants emitted by vehicles including CO, hydrocarbons (HCs), NO and NH_3, *etc.*[6−11] Although the study of Pt/Al_2O_3 catalysts has been ongoing for a long time, the increasing demand for better catalytic activity and developing characterization techniques are still driving researchers to design more efficient Pt/Al_2O_3 catalysts and gain a deeper understanding of the reaction mechanism.[12−16] Among the strategies for enhancing the catalytic performance of Pt/Al_2O_3 catalysts, fine-tuning the dispersion (or particle size) of Pt species has been found to be the most effective.[17−21] For instance, Haneda *et al.* prepared a series of Pt/Al_2O_3 catalysts with different Pt dispersion by controlling the calcination temperature. They found that the turnover frequency (TOF) of C_3H_6 oxidation on Pt/Al_2O_3 catalysts strongly depended on Pt dispersion, and Pt/Al_2O_3 with a high Pt dispersion of *ca.* 80% exhibited the highest C_3H_6 oxidation

Received: August 11, 2023
Revised: October 29, 2023
Accepted: December 5, 2023
Published: December 26, 2023

activity.[18] Slavinskaya *et al.* also fully investigated the impact of dispersion and the oxidation states of Pt species on their NH_3 oxidation activity. They revealed that large Pt particles with more Pt^0 species performed better in NH_3 oxidation reaction.[19] In the aspect of further increasing the Pt dispersion and constructing Pt single atoms on Al_2O_3 support, Kwak *et al.* reported that unsaturated pentacoordinate Al^{3+} (Al^{3+}_{penta}) centers on the (100) facets of the γ-Al_2O_3 surface could anchor isolated Pt atoms, which exhibited much better CO oxidation activity than Pt clusters/particles.[20] Zhang *et al.* also successfully prepared a Pt single-atom catalyst that was highly stable under CO oxidation atmosphere, using a mesoporous γ-Al_2O_3 support rich in coordinatively unsaturated pentahedral Al^{3+} centers.[21]

To the best of our knowledge, tuning the dispersion of Pt species has always required complex experimental operations or special supports, particularly using Al_2O_3 supports with rich Al^{3+}_{penta} centers.[22−24] Additionally, no systematic work has reported on tuning the Pt dispersion on Al_2O_3 support from single atoms to clusters/particles by a simple method while simultaneously revealing the intrinsic structure−activity relationship in different catalytic oxidation reactions. Inspired by our previous work on constructing Pt single atoms by impregnating Pt species on bayerite $Al(OH)_3$ support,[25] and the previous report that the surface hydroxyl groups significantly impacted the dispersion of various metal (or metal oxide) species,[26−29] in this work, a series of Pt/Al_2O_3 catalysts with different Pt dispersion states from single atoms to clusters (*ca.* 2 nm) were prepared by using bayerite $Al(OH)_3$ as support directly or precalcined at 200 or 550 °C. We found that the amount of hydroxyl groups on fresh and precalcined bayerite $Al(OH)_3$ support directly determined the dispersion of subsequent impregnated Pt species. Based on the results of catalytic performance evaluation in CO and NH_3 oxidation reactions as well as systematic characterizations, a clear structure−activity relationship of Pt/Al_2O_3 catalysts with different Pt dispersion states in these oxidation reactions was established.

2. EXPERIMENTAL SECTION

2.1. Catalyst Preparation. To tune the dispersion of Pt species on Al_2O_3, bayerite $Al(OH)_3$ support was used directly or precalcined at 200 or 550 °C, which was denoted as $Al(OH)_3$-F, $Al(OH)_3$-200, and $Al(OH)_3$-550, respectively (-F indicates fresh, and -200 and -550 indicate precalcination temperatures). $Pt(NO_3)_2$ was used as the Pt precursor, and the loading of Pt on Al_2O_3 was controlled at 1 wt % Pt/Al_2O_3 catalysts with different Pt dispersion states which were prepared by conventional incipient wetness impregnation (IWI) method, followed by calcination at 550 °C for 2 h. The Pt/Al_2O_3 catalysts, using $Al(OH)_3$-F, $Al(OH)_3$-200, and $Al(OH)_3$-550 as support, were denoted as Pt/Al_2O_3-H (-H = high dispersion), Pt/Al_2O_3-M (-M = medium dispersion), and Pt/Al_2O_3-L (-L = low dispersion), respectively. A detailed flowchart of the preparation process is demonstrated in Figure S1 to aid in better understanding.

2.2. Catalytic Performance Evaluation. The catalytic performance of the prepared Pt/Al_2O_3 catalysts in CO/NH_3 oxidation reactions was evaluated on a fixed-bed quartz tube reactor. For CO oxidation reaction, the feeding gas was composed of 1% CO, 5% O_2, and 5 vol % H_2O (when used), using Ar as balance. The concentration of CO in the outlet gas was analyzed by an online gas chromatograph (GC) instrument equipped with a thermal conduction detector (TCD) or an online mass spectrometer (MS). For NH_3 oxidation reaction, the feeding gas consisted of 500 ppm of NH_3, 5% O_2, and 5 vol % H_2O (when used), using Ar as balance. The concentrations of NH_3, NO, NO_2, and N_2O in the outlet gas were analyzed by using a Thermo Nicolet iS10 FTIR spectrometer equipped with a 2 m path-length gas cell (200 mL volume). In each test, the total flow rate was controlled at 100 mL·min^{-1}, and the usage of the catalyst was 30 mg, resulting in a weight hourly space velocity (WHSV) of 200,000 mL·g_{cat}^{-1}·h^{-1}. To minimize the heat effect, the catalyst was diluted with 300 mg of SiC for each test. Before the catalytic performance evaluation, all catalysts were pretreated in air flow at 300 °C for 30 min. CO conversion in CO oxidation reaction and NH_3 conversion and N_2 selectivity in NH_3 oxidation reaction were calculated according to the following equations:

$$\text{CO conversion (\%)} = \left(\frac{[CO]_{in} - [CO]_{out}}{[CO]_{in}}\right) \times 100\%$$

$$NH_3 \text{ conversion (\%)} = \left(\frac{[NH_3]_{in} - [NH_3]_{out}}{[NH_3]_{in}}\right) \times 100\%$$

$$N_2 \text{ selectivity (\%)} = \left(\frac{[NH_3]_{in} - [NH_3]_{out} - [NO]_{out} - [NO_2]_{out} - 2[N_2O]_{out}}{[NH_3]_{in} - [NH_3]_{out}}\right) \times 100\%$$

For kinetics study, the reaction rates were calculated with CO/NH_3 conversion below 20%, which could be controlled by tuning the WHSV and the reaction temperature.

2.3. Characterization. X-ray powder diffraction (XRD) patterns for the prepared catalysts were collected on a Philips X'pert Pro diffractometer, equipped with a Ni-filtered Cu Kα_1 radiation source (0.15406 nm). The collection range of 2θ was 15−85°, with a scan step of 0.02°. The scan speed was controlled at 10°·min^{-1}.

The N_2 adsorption−desorption isotherms measured on a Micromeritics ASAP 2020 analyzer at −196 °C were used to calculate the specific surface areas of the prepared catalysts, using the Brunauer−Emmett−Teller (BET) method. Before the measurement, the loaded catalysts were degassed at 300 °C in vacuum for 3 h.

X-ray photoelectron spectroscopy (XPS) experiments were conducted on a PHI 5000 Versa Probe system, which was equipped with an Al Kα source gun (1486.6 eV). C 1s at 284.6 eV was used to calibrate the binding energies of all elements. Before the measurement, the catalysts were placed in a vacuum chamber for 12 h.

X-ray absorption spectroscopy (XAS) for Pt L_3-edge of Pt/Al_2O_3 catalysts was measured at 7-BM QAS beamline of the National Synchrotron Light Source II (NSLS-II) at Brookhaven National Laboratory in fluorescence mode. The X-ray energies of this beamline range from 4.7 to 31 keV. The monochromator has a Si(111) channel-cut crystal and runs at a continuous scan mode. Demeter software package was used to analyze the XAS data including X-ray absorption near-edge structure (XANES) and extended X-ray absorption fine structure (EXAFS).

Atomic-resolution aberration-corrected high-angle annular dark field scanning transmission electron microscopic (AC-HAADF-STEM) images of Pt/Al_2O_3 catalysts were obtained on an FEI Titan Cubed G2 60-300 aberration-corrected S/TEM instrument. The accelerating voltage was controlled at 300 kV. The observations were performed in the HAADF mode to allow the Z-contrast imaging. The probe convergence angle on the Titan electron microscope was 22 mrad, and the angular range of the HAADF detector was from 79.5 to 200 mrad. The energy-dispersive spectroscopy (EDS) elemental mapping images in the STEM mode were collected on the Titan electron microscope using SuperX system.

Thermogravimetry and differential thermal analysis (TG-DTA) was conducted on a Netzsch thermoanalyzer STA 449C from room temperature to targeted temperatures (200, 550, or 900 °C) in flowing air with a temperature ramping rate of 5 °C·min^{-1}.

CO-temperature-programmed reduction (CO-TPR) experiment was performed on a fixed-bed quartz tube reactor, using an online mass spectrometer as a detector. In each test, 100 mg catalyst was loaded into the quartz tube and pretreated with purified air at 300 °C

https://doi.org/10.1021/acsami.3c11897
ACS Appl. Mater. Interfaces 2024, 16, 454−466

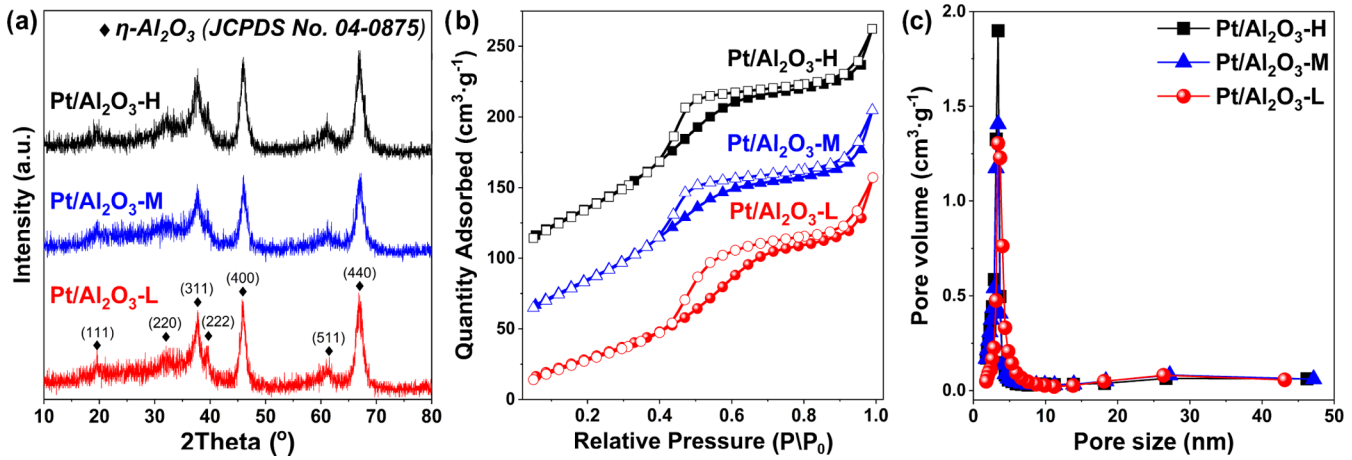

Figure 1. (a) XRD patterns, (b) nitrogen adsorption−desorption isotherms, and (c) BJH pore size distribution for Pt/Al_2O_3−H, Pt/Al_2O_3-M, and Pt/Al_2O_3-L catalysts.

Table 1. Data summary on N_2 Adsorption−Desorption, Raman Spectra, and XPS Analysis

			surface atomic concentration (%)[c]			
samples	BET SA ($m^2 \cdot g^{-1}$)[a]	pore volume ($cm^3 \cdot g^{-1}$)[b]	Al	O	Pt	Pt^{4+}/total Pt (%)[c]
Pt/Al_2O_3-H	268	0.30	33.0	63.8	3.2	100.0
Pt/Al_2O_3-M	246	0.28	34.8	62.5	2.8	100.0
Pt/Al_2O_3-L	189	0.28	30.8	66.8	2.4	90.0

[a]BET surface area (SA) was determined by N_2 adsorption−desorption isotherms measured at −196 °C. [b]The pore volume was determined by BJH method using desorption isotherms. [c]Surface atomic concentration and Pt^{4+}/total Pt were determined by XPS analysis.

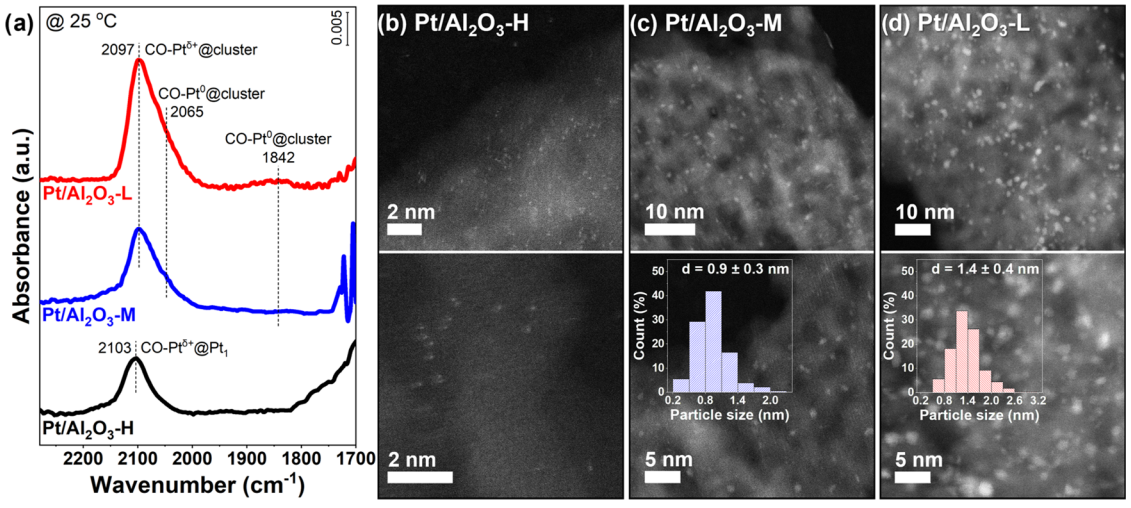

Figure 2. (a) *In situ* DRIFTS of CO adsorption on Pt/Al_2O_3-H, Pt/Al_2O_3-M, and Pt/Al_2O_3-L at 25 °C; AC-HAADF-STEM images of (b) Pt/Al_2O_3-H, (c) Pt/Al_2O_3-M, and (d) Pt/Al_2O_3-L (the Pt particle size distributions on Pt/Al_2O_3-M and Pt/Al_2O_3-L are shown in the inserted figures).

for 30 min and then cooled to room temperature. Afterwards, the loaded catalyst was exposed to a flow of 10% CO/Ar (30 mL·min^{-1}) and heated from 40 to 700 °C linearly with a ramping rate of 10 °C·min^{-1}.

In situ diffuse reflectance infrared Fourier transform spectroscopy (*in situ* DRIFTS) was performed on a Nicolet 5700 FTIR spectrometer using a mercury−cadmium−telluride (MCT) detector. The spectra were collected from 400 to 4000 cm^{-1} at a spectral resolution of 4 cm^{-1} for 64 scans or 16 scans (CO-TPR and CO/NH_3 adsorption/oxidation experiments). Prior to each test, the sample was pretreated with purified air at 300 °C for 0.5 h to remove the possibly adsorbed impurities (e.g., H_2O and CO_2) on catalysts. Then, the sample was cooled to targeted temperatures. The background spectrum was collected and subtracted from the recorded spectrum automatically. For *in situ* CO-TPR experiments, the feeding gas (50 mL·min^{-1}) consisted of 1% CO, using Ar as balance. For *in situ* CO adsorption/oxidation experiments, the feeding gas (50 mL·min^{-1}) consisted of 1% CO (when used) and/or 5% O_2 (when used), using Ar as balance. The ramping rate in both CO-TPR and CO oxidation experiments was controlled at 5 °C·min^{-1} (from 25 to 300 °C). For *in situ* NH_3 adsorption/oxidation experiments conducted at 210 or 220 °C, the feeding gas was composed of 500 ppm NH_3 (when used) and 5% O_2 (when used), using Ar as balance.

3. RESULTS AND DISCUSSION

3.1. Structural Information. XRD patterns for the as-prepared Pt/Al_2O_3 catalysts were first collected to investigate their crystal structure. As shown in Figure 1a, after the

https://doi.org/10.1021/acsami.3c11897
ACS Appl. Mater. Interfaces 2024, 16, 454−466

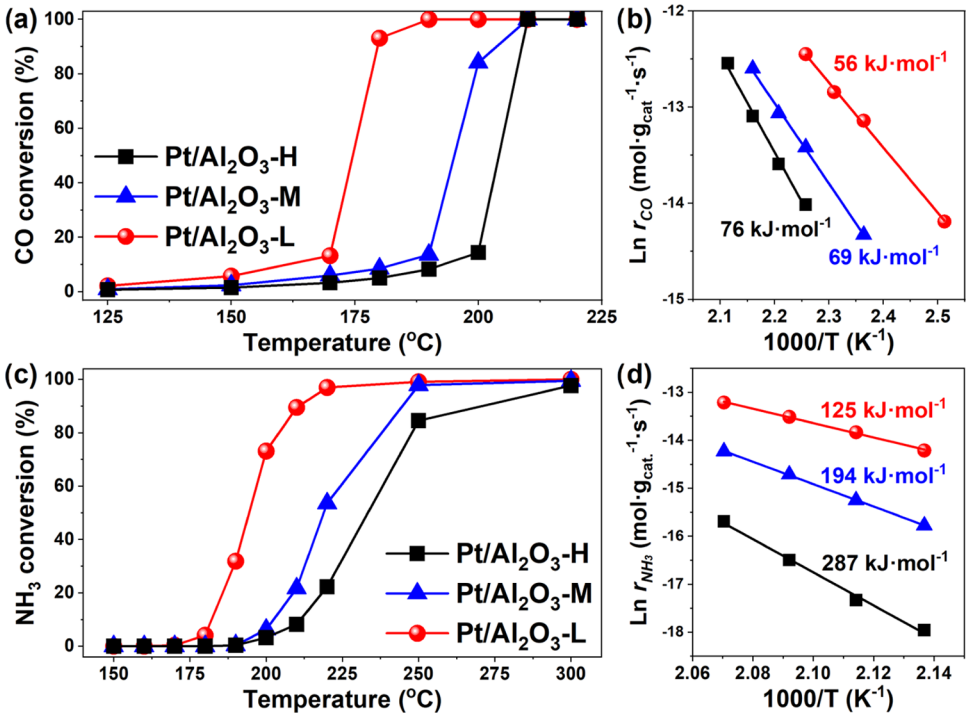

Figure 3. (a) CO oxidation activity on Pt/Al_2O_3-H, Pt/Al_2O_3-M, and Pt/Al_2O_3-L catalysts (Reaction conditions: 1% CO, 5% O_2, using Ar as balance, WHSV = 200,000 $mL{\cdot}g^{-1}{\cdot}h^{-1}$). (b) Apparent activation energy of CO oxidation reaction on Pt/Al_2O_3-H, Pt/Al_2O_3-M, and Pt/Al_2O_3-L catalysts (WHSV = 400,000 $mL{\cdot}g^{-1}{\cdot}h^{-1}$). (c) NH_3 oxidation activity on Pt/Al_2O_3-H, Pt/Al_2O_3-M, and Pt/Al_2O_3-L catalysts (Reaction conditions: 500 ppm NH_3, 5% O_2, using Ar as balance, WHSV = 200,000 $mL{\cdot}g^{-1}{\cdot}h^{-1}$). (d) Apparent activation energy of NH_3 oxidation reaction on Pt/Al_2O_3-H, Pt/Al_2O_3-M, and Pt/Al_2O_3-L catalysts (WHSV = 400,000 $mL{\cdot}g_{cat}^{-1}{\cdot}h^{-1}$ for Pt/Al_2O_3-H and Pt/Al_2O_3-M catalysts and 1,600,000 $mL{\cdot}g_{cat}^{-1}{\cdot}h^{-1}$ for Pt/Al_2O_3-L catalyst).

deposition of Pt and further calcination at 550 °C for 2 h, all XRD peaks on Pt/Al_2O_3 catalysts could be assigned to η-Al_2O_3 (JCPDS No. 04-0875). It should be noted that the XRD pattern for η-Al_2O_3 was quite similar to that of γ-Al_2O_3 (JCPDS No. 29-0063), and only slight differences in the intensity and peak width of XRD peaks were observed (Figure S2), indicating that both η-Al_2O_3 and γ-Al_2O_3 showed similar crystal structures. According to previous reports, the most notable difference between these two commonly used Al_2O_3 supports was that η-Al_2O_3 with the preferentially exposed (111) facet and γ-Al_2O_3 with the preferentially exposed (110) facet might show varied acidity and defect distribution.[30−32] The absence of XRD peaks assigned to the crystalline Pt or PtO_x indicated that all Pt species were well dispersed and below the detection limit of XRD. N_2-physisorption experiment was also conducted to measure the BET surface area (SA) and explore the pore structure of Pt/Al_2O_3 catalysts. As listed in Table 1, the BET SA of Pt/Al_2O_3-L (189 $m^2{\cdot}g^{-1}$) was relatively lower than that of Pt/Al_2O_3-M (246 $m^2{\cdot}g^{-1}$) and Pt/Al_2O_3-H (268 $m^2{\cdot}g^{-1}$), which could be resulted from the precalcination of bayerite $Al(OH)_3$ at a higher temperature (550 °C) before being used as the support for Pt/Al_2O_3-L. The N_2 adsorption−desorption isotherms and pore size distributions of the Pt/Al_2O_3 catalysts are demonstrated in Figure 1b,c. The isotherm profiles for all Pt/Al_2O_3 catalysts were found to exhibit a typical type II and type IV mixture, with an H4 hysteresis loop, suggesting the formation of narrow slit pores,[33] as confirmed by the results of pore size distributions.

3.2. Dispersion of Pt Species. To further investigate the dispersion of Pt species on Pt/Al_2O_3 catalysts, *in situ* DRIFTS of CO adsorption, a commonly used approach to explore the dispersion and oxidation states of platinum group metals (PGMs), was first conducted. As shown in Figure 2a, after being saturated with CO and purged by Ar, IR bands from 2000 to 2150 cm^{-1} were observed on Pt/Al_2O_3 catalysts which could be assigned to CO adsorbed on Pt sites in different states. For Pt/Al_2O_3-H, a highly symmetrical CO IR band centered at 2103 cm^{-1} was observed, which could be assigned to linearly adsorbed CO on isolated Pt ions (CO-$Pt^{\delta+}$@Pt_1),[34−36] indicating that the Pt species on Pt/Al_2O_3-H catalyst were mainly in the form of Pt single atoms. For Pt/Al_2O_3-M and Pt/Al_2O_3-L, the CO IR bands from 2000 to 2150 cm^{-1} could be an overlap of two sub-bands at *ca.* 2097 and 2065 cm^{-1}, which were related to CO linearly adsorbed on ionic Pt sites and Pt^0 sites on Pt/PtO_x clusters (CO-$Pt^{\delta+}$@cluster or CO-Pt^0@cluster), respectively.[21,36−38] The higher intensity of CO IR bands on Pt/Al_2O_3-L could have resulted from the easier CO adsorption on Pt/PtO_x clusters with a relatively larger size. Moreover, a broad band at 1842 cm^{-1} was observed on Pt/Al_2O_3-L, which could be assigned to bridge-bonded CO adsorbed on aggregated Pt species, further confirming that aggregated Pt species were formed on Pt/Al_2O_3-L.

To further evaluate the Pt dispersion on different Pt/Al_2O_3 catalysts, AC-HAADF-STEM images were collected. As shown in Figure 2b, for Pt/Al_2O_3-H, abundant bright dots were observed which could be assigned to the isolated Pt atoms on Al_2O_3 support, matching well with the result of *in situ* DRIFTS of CO adsorption. Different from Pt/Al_2O_3-H, the Pt species on Pt/Al_2O_3-M and Pt/Al_2O_3-L were found to aggregate into Pt/PtO_x clusters, and the Pt/PtO_x clusters on Pt/Al_2O_3-M were relatively smaller than those on Pt/Al_2O_3-L. To further evaluate the average size of Pt species on Pt/Al_2O_3-M and Pt/

https://doi.org/10.1021/acsami.3c11897
ACS Appl. Mater. Interfaces 2024, 16, 454−466

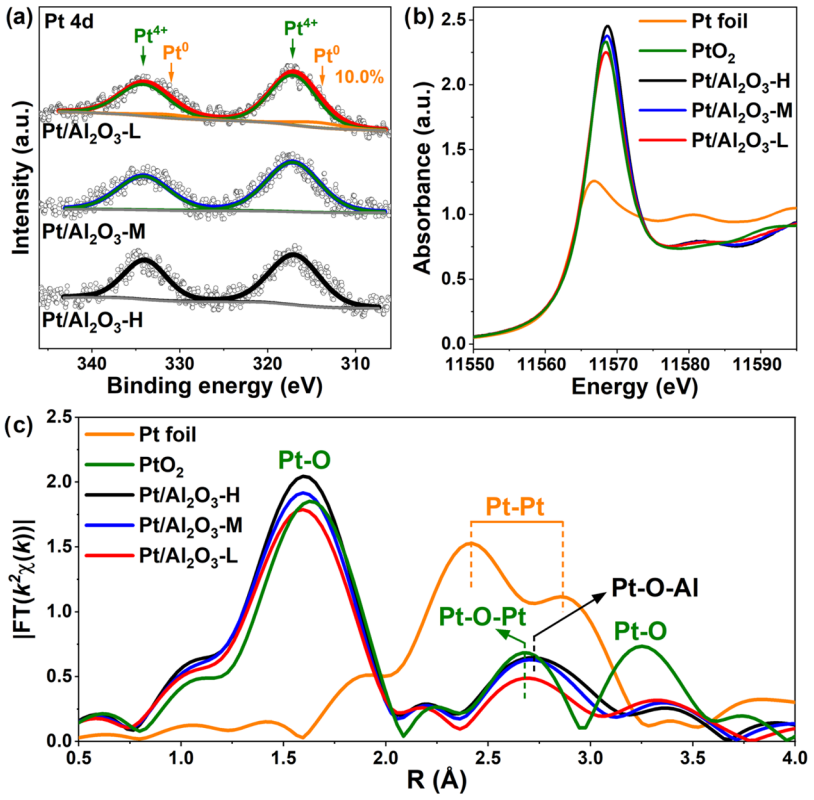

Figure 4. (a) Pt 4d XPS for Pt/Al_2O_3-H, Pt/Al_2O_3-M, and Pt/Al_2O_3-L catalysts. (b) Normalized XANES and (c) Fourier transformed k^2-weighted EXAFS oscillations in R space for Pt L_3-edge in Pt foil, PtO_2, Pt/Al_2O_3-H, Pt/Al_2O_3-M, and Pt/Al_2O_3-L catalysts.

Al_2O_3-L catalysts, a statistical analysis of cluster size distribution was conducted. According to the results of particle size distribution analysis, the average cluster size of Pt species within Pt/Al_2O_3-M (d = 0.9 ± 0.3 nm) was smaller than those within Pt/Al_2O_3-L (d = 1.4 ± 0.4 nm). The EDS-mapping images of Pt/Al_2O_3 catalysts were also collected to further investigate the dispersion of Pt species. As shown in Figure S3, no obvious aggregation of Pt species was observed on Pt/Al_2O_3-H, further confirming the high Pt dispersion on this catalyst that was in clear contrast with the monotonically decreased Pt dispersion on Pt/Al_2O_3-M and Pt/Al_2O_3-L. In short summary, as confirmed by the results of *in situ* DRIFTS of CO adsorption and AC-HAADF-STEM/EDS mapping, the Pt dispersion followed an order of Pt/Al_2O_3-H > Pt/Al_2O_3-M > Pt/Al_2O_3-L, as expected, and the Pt species on Pt/Al_2O_3-H catalyst were in the form of single atoms.

3.3. Catalytic Performance in CO and NH_3 Oxidation Reactions. The catalytic performance of Pt/Al_2O_3 catalysts with different Pt dispersion states in CO and NH_3 oxidation, two common but important reactions in vehicle emission control, was evaluated in this study. As shown in Figure 3a, the CO oxidation activity on Pt/Al_2O_3 catalysts followed the sequence of Pt/Al_2O_3-L > Pt/Al_2O_3-M > Pt/Al_2O_3-H, suggesting that Pt/Al_2O_3 catalysts with relatively lower Pt dispersion could perform better in CO oxidation reaction. The CO reaction rate at 170 °C was also calculated (Figure S4). Pt/Al_2O_3-L (39 $\mu mol \cdot g_{cat.}^{-1} \cdot s^{-1}$) was found to exhibit a much higher CO oxidation rate than Pt/Al_2O_3-M (16 $\mu mol \cdot g_{cat.}^{-1} \cdot s^{-1}$) and Pt/Al_2O_3-H (7 $\mu mol \cdot g_{cat.}^{-1} \cdot s^{-1}$). Further kinetics study revealed that the apparent activation energy (E_a) of CO oxidation reaction on Pt/Al_2O_3-L (56 $kJ \cdot mol^{-1}$) was lower than that on Pt/Al_2O_3-M (69 $kJ \cdot mol^{-1}$) and Pt/Al_2O_3-H (76 $kJ \cdot mol^{-1}$) (Figure 3b), suggesting that CO and O_2 could be better activated on Pt/Al_2O_3-L.

Similar to the activity sequence observed in CO oxidation reaction, as illustrated in Figures 3c and S5, Pt/Al_2O_3-L also exhibited much higher NH_3 oxidation activity than Pt/Al_2O_3-M and Pt/Al_2O_3-H. The NH_3 oxidation rate at 200 °C on Pt/Al_2O_3-L (0.98 $\mu mol \cdot g_{cat.}^{-1} \cdot s^{-1}$) was 4 and 33 times of that on Pt/Al_2O_3-M (0.24 $\mu mol \cdot g_{cat.}^{-1} \cdot s^{-1}$) and Pt/Al_2O_3-H (0.03 $\mu mol \cdot g_{cat.}^{-1} \cdot s^{-1}$), respectively. The much lower E_a of NH_3 oxidation reaction on Pt/Al_2O_3-L (125 $kJ \cdot mol^{-1}$) than that on Pt/Al_2O_3-M (194 $kJ \cdot mol^{-1}$) and Pt/Al_2O_3-H (287 $kJ \cdot mol^{-1}$) further suggested that NH_3 could be activated and oxidized easily on Pt/Al_2O_3 catalysts with relatively lower Pt dispersion (Figure 3d). Furthermore, although Pt/Al_2O_3-L catalyst showed much higher NH_3 oxidation activity than Pt/Al_2O_3-H and Pt/Al_2O_3-M, the N_2 selectivity achieved on Pt/Al_2O_3-L was still comparable to that on Pt/Al_2O_3-M and Pt/Al_2O_3-H (Figure S6), suggesting the promising potential of Pt/Al_2O_3-L catalyst for practical application. The concentrations of N_2O, NO, and NO_2 generated during the catalytic performance evaluation were also plotted and shown in Figure S7.

Long-term activity evaluations were conducted on Pt/Al_2O_3 catalysts to evaluate their stability. In both CO oxidation reaction (190 °C) and NH_3 oxidation reaction (200 °C), limited change was observed on all Pt/Al_2O_3 catalysts throughout the test (Figures S8 and S9), suggesting their superior stability at a fixed reaction temperature. Three-round cycling CO/NH_3 oxidation test was also performed from 30 to 300 °C for each catalyst to further evaluate the catalytic stability. As shown in Figures S10 and S11, no decrease but only a slight increase in the activity was observed after three-round tests for all catalysts in CO oxidation and NH_3 oxidation

https://doi.org/10.1021/acsami.3c11897
ACS Appl. Mater. Interfaces 2024, 16, 454−466

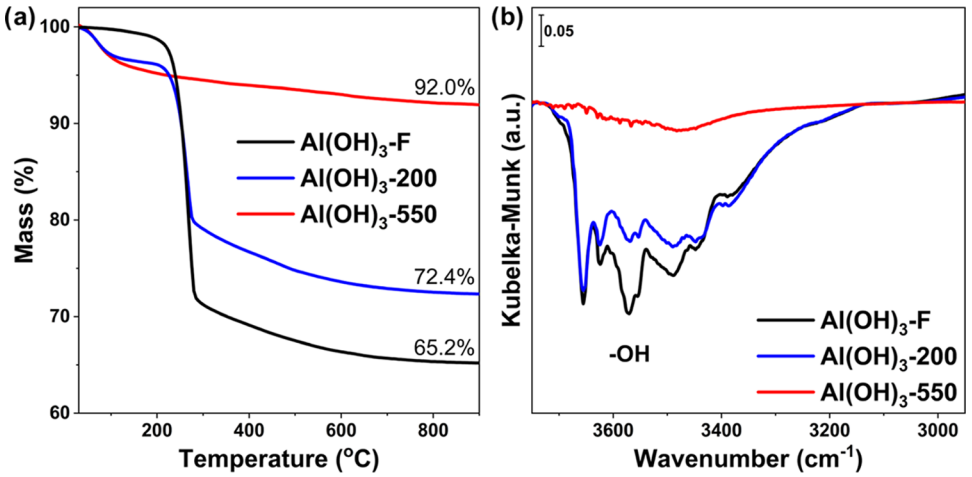

Figure 5. (a) TG profiles for $Al(OH)_3$-F, $Al(OH)_3$-200, and $Al(OH)_3$-550. (b) *In situ* DRIFTS of dehydration on $Al(OH)_3$-F, $Al(OH)_3$-200, and $Al(OH)_3$-550.

reactions, indicating the satisfying stability of Pt/Al_2O_3 catalysts. Under practical application conditions, the presence of abundant H_2O in the vehicle exhaust could also show a significant impact on the performance of aftertreatment catalyst systems. Taking this into consideration, the catalytic performance of Pt/Al_2O_3 catalysts in the presence of H_2O was also evaluated. As shown in Figure S12, after the introduction of H_2O into the feeding gas, Pt/Al_2O_3-L still performed much better than Pt/Al_2O_3-M and Pt/Al_2O_3-H in both CO oxidation and NH_3 oxidation reactions. Interestingly, it was found that the CO oxidation activity on Pt/Al_2O_3 catalysts was even enhanced by the addition of H_2O, which could be resulted from the more efficient activation of oxygen species as well as the direct reaction between CO and hydroxyl groups.[39,40] Although H_2O had some inhibitory effect on the NH_3 oxidation activity over Pt/Al_2O_3 catalysts, with the increase of 8−15 °C in T_{50} (T_{50} = the temperature at which the conversion reached 50%), Pt/Al_2O_3-L catalyst still performed much better than Pt/Al_2O_3-M and Pt/Al_2O_3-H under wet conditions (Figure S13).

3.4. Oxidation States of Pt Species on Pt/Al_2O_3 Catalysts. Besides the Pt dispersion, the oxidation state of Pt species was another important factor determining their catalytic performance. Therefore, Pt 4d XPS were measured first for Pt/Al_2O_3 catalysts, and the results are shown in Table 1 and Figure 4a. After peak deconvolution, it was found that the Pt species on Pt/Al_2O_3 catalysts were mainly in the form Pt^{4+}, and only a small amount of Pt^0 species (10.0%) were observed on Pt/Al_2O_3-L. No significant difference was observed for Al 2p and O 1s XPS on Pt/Al_2O_3-H, Pt/Al_2O_3-M, and Pt/Al_2O_3-L (Figure S14), indicating that Al and O species on all catalysts were in similar states. The surface atomic concentrations of all elements were also calculated and listed in Table 1. Moreover, the monotonically decreased atomic concentrations of Pt observed on Pt/Al_2O_3-H (3.2%), Pt/Al_2O_3-M (2.8%), and Pt/Al_2O_3-L (2.4%) further confirmed that different dispersion states of Pt species associated with varied oxidation states could be achieved on Pt/Al_2O_3 catalysts through the simple synthesis method as reported herein.

To further evaluate the valence states and local coordination structures of Pt species on Pt/Al_2O_3 catalysts, XAS analysis was performed. The normalized Pt L_3-edge XANES are illustrated in Figure 4b, using Pt foil and PtO_2 as references. The white line intensity of Pt L_3-edge XANES for Pt/Al_2O_3 catalysts followed a decreasing order of Pt/Al_2O_3-H > Pt/Al_2O_3-M > Pt/Al_2O_3-L, indicating the gradual decrease in the valence states of Pt species with decreased Pt dispersion from high to medium to low.[41,42] To obtain more accurate average valence states of Pt species on Pt/Al_2O_3 catalysts, XANES linear combination fitting was performed (Figure S15), and the calculated average valence states of Pt are listed in Table S1. As expected, the valence states of Pt followed the decreasing order of Pt/Al_2O_3-H > Pt/Al_2O_3-M > Pt/Al_2O_3-L, matching well with the Pt 4d XPS results as discussed above. The first-order derivatives of Pt L_3-edge XANES for Pt/Al_2O_3 serial catalysts also supported the above conclusion as the absorption edge energies of Pt L_3-edge followed the same trend of Pt/Al_2O_3-H > Pt/Al_2O_3-M > Pt/Al_2O_3-L (Figure S16).

The Fourier transformed k^2-weighted EXAFS oscillations in R space are plotted and shown in Figure 4c, and the curve fitting results can be found in Figure S17 and Table S2. Within all Pt/Al_2O_3 catalysts, Pt−O coordination shells were observed and the coordination numbers (CNs) of Pt−O followed the sequence of Pt/Al_2O_3-H (6.3) > Pt/Al_2O_3-M (6.0) > Pt/Al_2O_3-L (5.7), which were consistent with the monotonically decreased Pt valence states as determined by Pt 4d XPS and Pt L_3-edge XANES. For Pt/Al_2O_3-H catalyst, the absence of Pt−Pt/Pt−O−Pt coordination shells and the inclusive presence of Pt−O−Al coordination shell suggested that the Pt species in this catalyst were in the form of Pt single atoms, in good accordance with the *in situ* DRIFTS of CO adsorption and AC-HAADF-STEM results (Figure 2). For Pt/Al_2O_3-M catalyst, the second coordination shell was mainly composed of Pt−O−Al with slightly lowered CN (4.7) than that in Pt/Al_2O_3-H (5.0), but could not exclude the contribution from Pt−O−Pt (although the curve fitting of the second coordination shell in Pt/Al_2O_3-M was only performed using Pt−O−Al scattering pathway to reduce complexity). For Pt/Al_2O_3-L catalyst, the discernible Pt−O−Pt coordination shell was clearly observed, confirming the formation of relatively larger PtO_x clusters within this catalyst. Although the Pt−O−Al interaction on Pt/Al_2O_3-M and Pt/Al_2O_3-H could be well proved by the results of XAS analysis, similar states of Al and O on all Pt/Al_2O_3 catalysts were demonstrated by XPS experiments (Figure S14). This should be due to the fact that the slight shift in the XPS peaks, if any, resulted from the electron transfer between the Pt

https://doi.org/10.1021/acsami.3c11897
ACS Appl. Mater. Interfaces 2024, 16, 454−466

species and Al_2O_3 support might be covered up by the XPS signals of those Al and O species without any interaction with Pt species, since the surface concentrations of Al (*ca.* 32%) and O (*ca.* 65%) were much higher than that of Pt (*ca.* 3%). Considering the much higher CO/NH_3 oxidation activity achieved on Pt/Al_2O_3-L catalyst than on others, it can be inferred that the PtO_x clusters on Pt/Al_2O_3 catalysts with relatively lower Pt dispersion and lower oxidation states could better catalyze the activation of O_2, CO, and NH_3.

3.5. Pt Dispersion Determined by the Concentration of Hydroxyls on Al_2O_3 Supports. As discussed above, higher Pt dispersion could be achieved when $Al(OH)_3$-F and $Al(OH)_3$-200 were used as Al_2O_3 support precursors. Therefore, it can be inferred that more hydroxyl groups on $AlO_x(OH)_y$ should be able to facilitate the higher dispersion of Pt species. To determine the amount of hydroxyl groups on $AlO_x(OH)_y$, TG experiments (from room temperature to 900 °C) were first conducted. As shown in Figure 5a, a weight loss of *ca.* 34.8% was observed on $Al(OH)_3$-F after heating up to 900 °C, which was almost identical to the theoretical weight loss (34.6%) for the complete decomposition of $Al(OH)_3$ to Al_2O_3 ($2Al(OH)_3 \rightarrow Al_2O_3 + 3H_2O$). For $Al(OH)_3$-200 and $Al(OH)_3$-550, due to the precalcination already completed at 200 and 550 °C for 2 h before TG experiments, the weight loss decreased to 27.6 and 8.0%, respectively. Based on these TG analysis results, the composition of $Al(OH)_3$-200 and $Al(OH)_3$-550 could be calculated and represented as $AlO_{0.42}(OH)_{2.16}$ and $AlO_{1.25}(OH)_{0.50}$, respectively. The precalcination process of bayerite $Al(OH)_3$ support was also simulated by TG-DTA experiments. As shown in Figure S18, the weight loss of fresh bayerite $Al(OH)_3$ after calcination at 550 °C (33.8%) was much higher than that after calcination at 200 °C (11.7%), further suggesting that the amount of −OH groups on $AlO_x(OH)_y$ supports followed a decreasing order of $Al(OH)_3$-F > $Al(OH)_3$-200 > $Al(OH)_3$-550.

To better demonstrate the dehydration process of bayerite $Al(OH)_3$, *in situ* DRIFTS experiments were designed. Before tests, $Al(OH)_3$-F, $Al(OH)_3$-200, and $Al(OH)_3$-550 were first pretreated under N_2 at 120 °C for 2 h, and then the background spectra were collected and automatically subtracted. Afterwards, the samples were heated to 550 °C and kept for 2 h. After cooling down in N_2 flow to 120 °C, the spectra for the dehydrated samples were collected. As clearly shown in Figure 5b, broad negative bands at 3100−3600 cm^{-1} assigned to −OH stretching vibration modes could be observed on all three supports.[43,44] However, the negative bands on $Al(OH)_3$-F and $Al(OH)_3$-200 showed much higher intensity than those on $Al(OH)_3$-550, suggesting the occurrence of more vigorous dehydration processes on the former two samples. These results show that $Al(OH)_3$-F and $Al(OH)_3$-200 possessed higher density of hydroxyl groups than $Al(OH)_3$-550, which were highly consistent with the TG-DTA results (Figures 5a and S18). Since Pt species were deposited onto the supports through IWI method, the hydrated Pt ions (e.g., $Pt(OH)_m(H_2O)_n$[45]) in aqueous solution could interact with hydroxyl groups on $AlO_x(OH)_y$ supports through hydrogen bonding, and more surface hydroxyl groups on $AlO_x(OH)_y$ supports could better promote the initial dispersion of $Pt(OH)_m(H_2O)_n$ species. After further calcination, strong Pt−O−Al bonds could be formed, and the concentration of hydroxyl groups on $AlO_x(OH)_y$ supports determined the final dispersion of Pt species on Pt/Al_2O_3 catalysts.[27,46] The anchoring process of Pt species on $AlO_x(OH)_y$ supports is shown in Scheme 1.

Scheme 1. Interaction between Hydrated Pt Ions and Surface Hydroxyl Groups on $AlO_x(OH)_y$ Supports

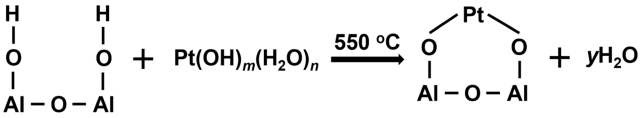

3.6. Interaction between CO and Pt/Al_2O_3 Catalysts Determined by CO-TPR. As mentioned in the catalytic performance section (Section 3.3), Pt/Al_2O_3-L exhibited much higher CO oxidation activity than Pt/Al_2O_3-M and Pt/Al_2O_3-H, suggesting that the interaction between CO and Pt species with varied dispersion on Al_2O_3 support should be significantly different. To evaluate the reducibility of Pt/Al_2O_3 catalysts and the surface structural evolution of Pt species driven by CO, *in situ* DRIFTS of CO-TPR experiment was designed, during which the CO consumption and the CO adsorption on Pt sites could be monitored simultaneously. As shown in Figures 6 and S19, with the increase of the reduction temperature from 30 to 300 °C, the intensity of the bands assigned to gaseous CO (*ca.* 2172 cm^{-1}) on Pt/Al_2O_3-H, Pt/Al_2O_3-M, and Pt/Al_2O_3-L decreased gradually, indicating the higher consumption rate of CO at increased temperature. Regarding the CO adsorption on Pt sites, strikingly distinct features were observed on different Pt/Al_2O_3 catalysts. On Pt/A_2O_3-H, an increase in the reduction temperature to around 140 °C or higher resulted in the prominent appearance of the band attributed to the CO-Pt^0@cluster species at approximately 2065 cm^{-1} (Figures 6a and S19a). This indicated the formation of aggregated Pt species with metallic Pt (Pt^0) sites. In clear contrast, the temperatures at which abundant CO-Pt^0@cluster species were formed on Pt/Al_2O_3-M (120 °C) and Pt/Al_2O_3-L (80 °C) were much lower than that on Pt/Al_2O_3-H (140 °C) (Figures 6b,c and S19b,c), suggesting that the oxygen species on PtO_x clusters/particles could react with CO more efficiently at lower temperatures than those near Pt single atoms. It was also found that the IR band intensity for CO-Pt^0@clusters on Pt/Al_2O_3-L was much more intensive than that on Pt/Al_2O_3-M and Pt/Al_2O_3-H, indicating that more Pt^0 sites on the surface of larger PtO_x clusters/particles could be formed on Pt/Al_2O_3-L during the CO reduction process. Considering the higher Pt dispersion on Pt/Al_2O_3-H and Pt/Al_2O_3-M than on Pt/Al_2O_3-L, it can be concluded that the $Pt^{\delta+}$ sites on the surface of relatively larger PtO_x clusters/particles could be reduced more easily, providing more Pt^0@cluster sites to adsorb CO in the bridge-type configuration (*ca.* 2065 cm^{-1}).

To further investigate the reducibility of Pt/Al_2O_3 catalysts and the Pt−Al_2O_3 interaction, conventional CO-TPR experiments were also conducted within a broader range of reduction temperature (30−700 °C). As shown in Figure 6d, besides the weak CO-consumption peaks at 100−250 °C attributed to the reduction of active oxygen species linked to Pt sites (α for Pt−O−Pt and α' for Pt−O), much broader and more intensive CO-consumption peaks were observed at higher temperatures (>300 °C), which could be assigned to the reduction of PtO_x species strongly interacting with Al_2O_3 support (β, Pt−O−Al).[46] It was observed that the center of peak β on Pt/Al_2O_3-H was located at a higher temperature (490 °C) compared to that on Pt/Al_2O_3-M (405 °C) and Pt/Al_2O_3-L (397 °C). This

https://doi.org/10.1021/acsami.3c11897
ACS Appl. Mater. Interfaces 2024, 16, 454−466

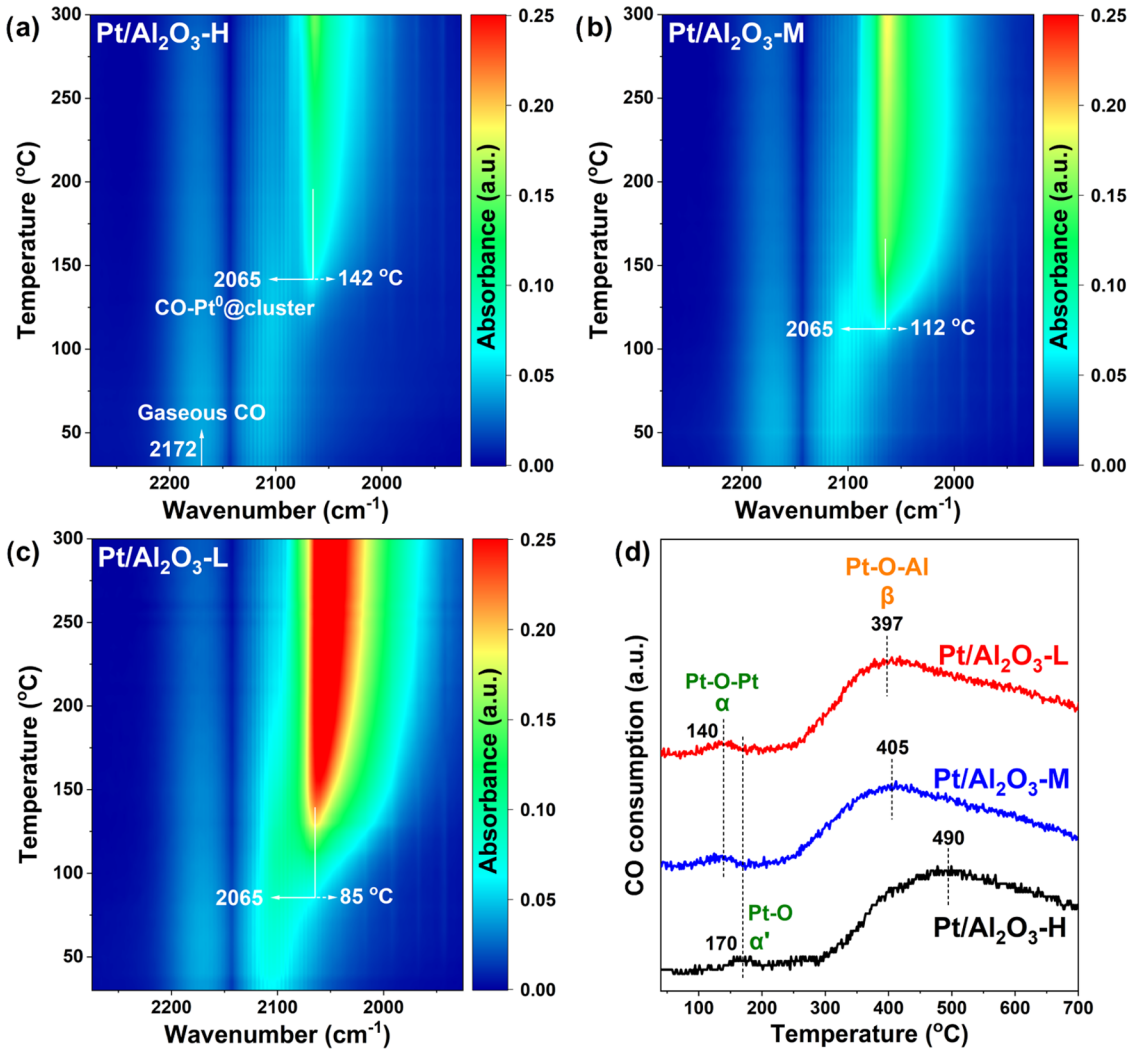

Figure 6. *In situ* DRIFTS of CO-TPR on (a) Pt/Al_2O_3-H, (b) Pt/Al_2O_3-M, and (c) Pt/Al_2O_3-L (Reaction conditions: 50 mg catalysts, 1% CO, using Ar as balance, total flow rate of 50 mL·min^{-1}). (d) CO-TPR profiles of Pt/Al_2O_3-H, Pt/Al_2O_3-M, and Pt/Al_2O_3-L.

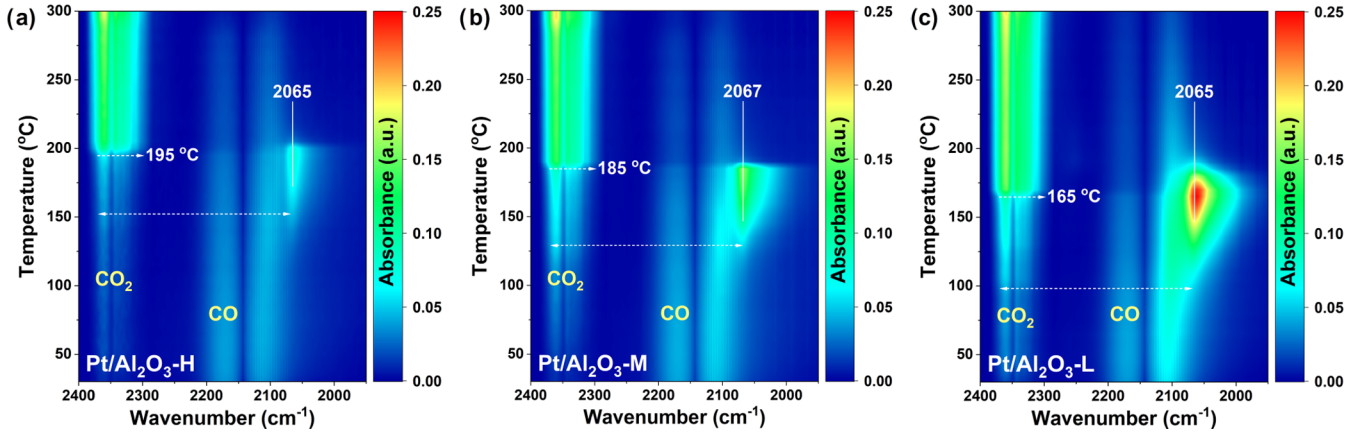

Figure 7. *In situ* DRIFTS of CO oxidation on (a) Pt/Al_2O_3-H, (b) Pt/Al_2O_3-M, and (c) Pt/Al_2O_3-L. Reaction conditions: 50 mg of catalysts, 1% CO, 5% O_2, using Ar as balance, and a total flow rate of 50 mL·min^{-1}.

finding further supports the viewpoint that stronger Pt−O−Al interaction was achieved on Pt/Al_2O_3-H due to the reaction between hydrated Pt ions ($Pt(OH)_m(H_2O)_n$) and abundant hydroxyl groups on $Al(OH)_3$-F support. Modulating the concentration of surface hydroxyls on $AlO_x(OH)_y$ supports could not only fine-tune the Pt dispersion on Al_2O_3 but also influence the reducibility of Pt species and the CO adsorption behavior.

3.7. Reaction Mechanism Study for CO and NH_3 Oxidation. To better reveal the structure−activity relationship

https://doi.org/10.1021/acsami.3c11897
ACS Appl. Mater. Interfaces 2024, 16, 454−466

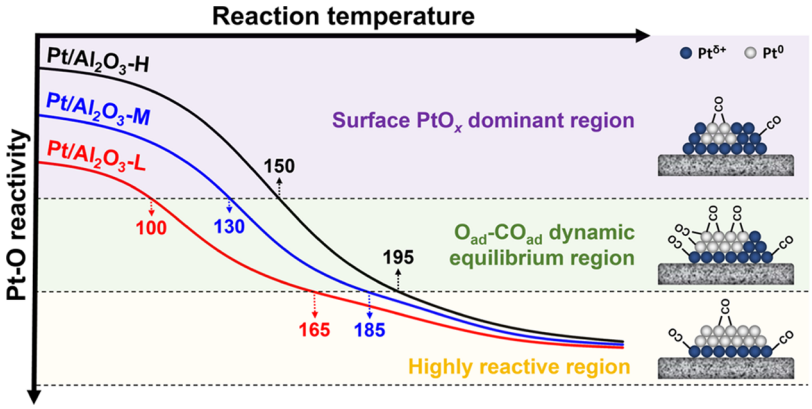

Figure 8. Reaction of temperature-dependent Pt−O reactivity on Pt/Al_2O_3 serial catalysts.

of Pt/Al_2O_3 catalysts, *in situ* DRIFTS experiments of CO oxidation were first performed. As shown in Figures 7 and S20, different from the results observed in CO-TPR experiments, when O_2 was also present in the feeding flow, the generation of abundant CO-Pt^0@cluster species (*ca.* 2065 cm^{-1}) on Pt/Al_2O_3 catalysts occurred at higher temperatures, suggesting that the surface reduction of PtO_x species was inhibited to a certain extent by O_2. More interestingly, a sharp increase in CO_2 concentration and decrease in CO concentration were observed simultaneously on Pt/Al_2O_3-H, Pt/Al_2O_3-M, and Pt/Al_2O_3-L at 195, 185, and 165 °C, respectively (Figures 7, S20, and S21), matching well with the sequence of light-off temperatures in CO oxidation on Pt/Al_2O_3 catalysts as observed in Figure 3a. It was also found that the generation of CO_2 coincided with the formation of CO-Pt^0@clusters, indicating that the Pt^0 species formed on the surface of PtO_x clusters/particles under the reaction condition were the most active sites for CO oxidation. Additionally, the intensity of the bands assigned to CO-Pt^0@clusters decreased rapidly after the temperature at which the concentration of CO_2 sharply increased. Considering that the CO-Pt^0@cluster species could still be observed on Pt/Al_2O_3 catalysts during *in situ* DRIFTS of CO-TPR experiments even at a high temperature of 300 °C, it can be concluded that the gaseous O_2 could be efficiently activated by Pt^0@cluster sites and react vigorously with the adsorbed CO when the reaction temperature was higher than the light-off temperature.

As discussed above, the adsorption of CO on Pt^0@cluster sites was closely related to the reduction of PtO_x to Pt^0 by CO, *i.e.*, the removal of oxygen species coordinated to Pt, while O_2 could inhibit the formation of Pt^0@clusters to a certain extent. Therefore, it can be concluded that the competitive adsorption between CO and oxygen species on Pt sites, along with further activation of CO-Pt^0@cluster species and gaseous O_2, was found to be the crucial factor determining the CO oxidation activity on Pt/Al_2O_3 catalysts. In the case of Pt/Al_2O_3-L with relatively lower Pt dispersion, more $Pt^{\delta+}$ species on the surface of larger PtO_x clusters could be reduced to Pt^0 more easily at lower temperatures under the CO oxidation reaction condition. More notably, the activation of O_2 in the presence of CO on larger Pt^0@clusters was also easier, resulting in the lower temperature required for the light-off of CO oxidation on Pt/Al_2O_3-L catalyst (*i.e.*, 165 °C, Figure 7c).

After being exposed to CO oxidation flow at 300 °C for 30 min, the Pt/Al_2O_3 catalysts were cooled to 30 °C in the same flow without exposure to air. Thereafter, the IR spectra of CO + O_2 adsorption on Pt/Al_2O_3 catalysts were collected (Figure S22). It was observed that significantly more CO-Pt^0@cluster species remained on Pt/Al_2O_3-L, further suggesting that more Pt sites for CO adsorption were formed on this catalyst under the CO oxidation condition. The presence of a relatively weaker CO-Pt^0@cluster band on the used Pt/Al_2O_3-H suggested that a small portion of Pt single atoms on this catalyst had aggregated into small Pt/PtO_x clusters, which should be the main reason for the slightly improved CO oxidation activity on Pt/Al_2O_3-H during the cycling CO oxidation test (Figure S10). Nevertheless, Pt/Al_2O_3-H still exhibited the highest Pt dispersion compared to Pt/Al_2O_3-M and Pt/Al_2O_3-L after the CO oxidation reaction.

To better illustrate the dynamic change of Pt surface states and the surface adsorption characteristics of Pt/Al_2O_3 catalysts under CO oxidation condition, a summary scheme was proposed (Figure 8). When the reaction temperature was lower than 100, 130, or 150 °C for Pt/Al_2O_3-L, Pt/Al_2O_3-M, or Pt/Al_2O_3-H, respectively, the Pt−O species within PtO_x clusters or Pt−O−Al structures showed low reactivity toward CO and inhibited the adsorption of CO (*i.e.*, surface PtO_x dominant region). With further increase in reaction temperature, the reactivity of Pt−O species increased, thus generating more Pt^0@clusters for the easier adsorption and activation of CO and resulting in the enhanced CO oxidation activity (*i.e.*, O_{ad}−CO_{ad} equilibrium region). As the reaction temperature reached 165, 180, or 190 °C for Pt/Al_2O_3-L, Pt/Al_2O_3-M, and Pt/Al_2O_3-H, respectively, gaseous O_2 could be efficiently activated by Pt^0@clusters and the reactivity of residual Pt−O species toward CO could be enhanced significantly, contributing to the sharp increase in the CO oxidation activity (*i.e.*, highly reactive region). Since the Pt^0@clusters generated by the *in situ* reduction of $Pt^{\delta+}$ species on the surface of PtO_x clusters under the CO oxidation reaction flow were the intrinsic active sites for CO depletion, the more facile activation of $Pt^{\delta+}$ sites on larger PtO_x clusters to Pt^0@clusters on Pt/Al_2O_3-L catalyst at lower temperature was responsible for its much higher CO oxidation activity.

The reaction mechanism of NH_3 oxidation on Pt/Al_2O_3 catalysts was also investigated using *in situ* DRIFTS experiments. As shown in Figure 9, after being saturated with NH_3 at 210 °C, different NH_3 species were observed on Pt/Al_2O_3 catalysts. On all Pt/Al_2O_3 catalysts, the IR bands at *ca.* 1259−1262 and 1228−1234 cm^{-1} could be assigned to the NH_3 adsorbed on Lewis acid sites (NH_3-L).[47−49] The IR bands assigned to NH_4^+ species coordinated to Brønsted acid sites

https://doi.org/10.1021/acsami.3c11897
ACS Appl. Mater. Interfaces 2024, 16, 454−466

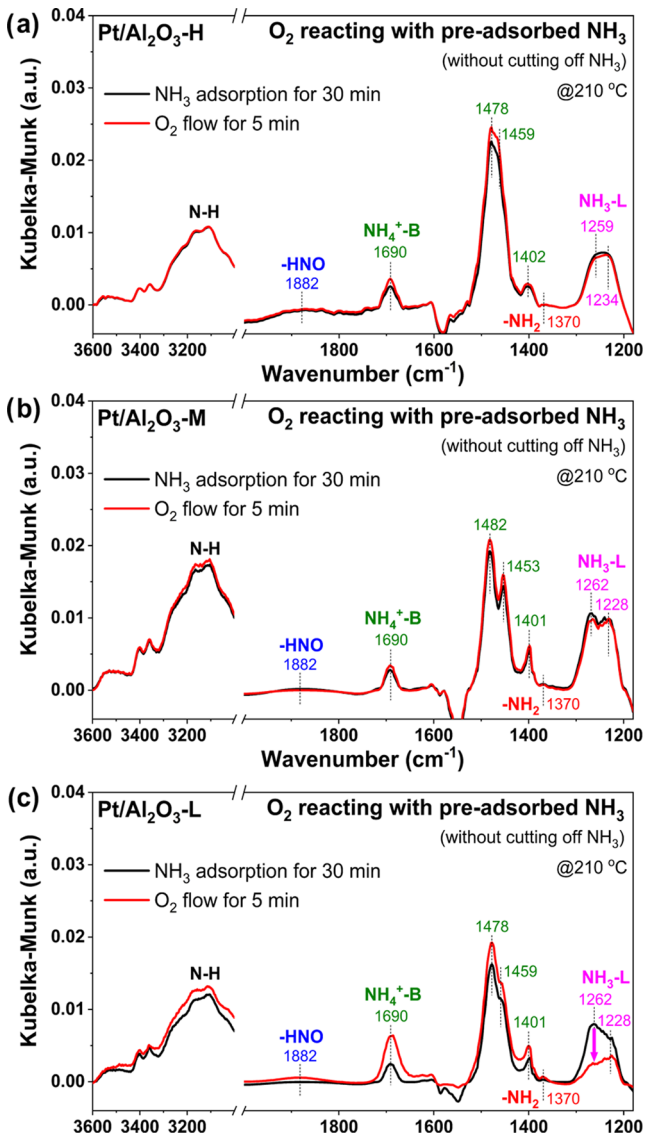

Figure 9. *In situ* DRIFTS of O_2 reacting with preadsorbed NH_3 on (a) Pt/Al_2O_3-H, (b) Pt/Al_2O_3-M, and (c) Pt/Al_2O_3-L catalysts at 210 °C.

(NH_3-B) were also observed at *ca.* 1690, 1478−1482, 1453−1459, and 1402 cm^{-1}.[50−52] The broad bands located at 3000−3500 cm^{-1} were attributed to the N−H stretching vibration modes of various NH_3 species.[51−53] The weak IR band at *ca.* 1370 cm^{-1} and the broad IR band at *ca.* 1882 cm^{-1} could be assigned to -NH_2 species and -HNO species, respectively, which should be generated by the dehydrogenation and activation of NH_3 adsorbed on Pt sites.[54−57] The comparable intensity of the IR bands assigned to adsorbed NH_3 species on Pt/Al_2O_3-H, Pt/Al_2O_3-M, and Pt/Al_2O_3-L suggested that the amount of surface acid sites was not a key factor determining their NH_3 oxidation activity.

To further investigate the reactivity of the adsorbed NH_3 species, O_2 was introduced into the feeding stream without cutting off NH_3. Different from the observation that the intensity of the IR bands assigned to adsorbed NH_3 species on Pt/Al_2O_3-H and Pt/Al_2O_3-M showed very limited change after the introduction of O_2 for 5 min at 210 °C (Figure 9a,b), the intensity of the IR bands assigned to NH_3-L species on Pt/Al_2O_3-L decreased significantly upon O_2 introduction (Figure 9c). These results suggested that the NH_3-L species on Pt/Al_2O_3-L catalyst could be activated more efficiently and then react with O_2. Meanwhile, the intensity of the bands assigned to NH_4^+-B species on Pt/Al_2O_3-L was enhanced, which could be resulted from the generation of H_2O through NH_3 oxidation and the subsequent formation of more surface hydroxyl groups serving as Brønsted acid sites. The intensity of the negative bands at *ca.* 1550 cm^{-1} related to the consumption of surface −OH groups by NH_3 adsorption also showed an obvious decrease in intensity (or recovery),[47,58] well supporting the viewpoint that hydroxyl groups were reproduced on Pt/Al_2O_3-L catalyst due to its efficient NH_3 oxidation capability. It was also noteworthy that more -NH_2 and -HNO species were formed on Pt/Al_2O_3-L after the introduction of O_2, further indicating that the NH_3 species on Pt/Al_2O_3-L catalyst were more reactive toward O_2, and -NH_2 and -HNO were important reaction intermediates during this process. With the reaction temperature increased to 220 °C (Figure S23), the NH_3-L species on Pt/Al_2O_3-M were found to be more reactive than those on Pt/Al_2O_3-H, supporting the observation in Figure 3c that Pt/Al_2O_3-M showed higher NH_3 oxidation activity than Pt/Al_2O_3-H.

Based on the results of *in situ* DRIFTS study, the main steps of NH_3 oxidation on Pt/Al_2O_3 catalysts in this work can be proposed as below:

$$NH_3 + O \rightarrow - NH_2 + - OH \quad (1)$$

$$-NH_2 + O \rightarrow - NH + - OH \quad (2)$$

$$-NH + O \rightarrow - HNO + - OH \quad (3)$$

$$-NH + - HNO \rightarrow N_2 + H_2O \quad (4)$$

$$2\text{-}HNO \rightarrow N_2O + H_2O \quad (5)$$

The more efficient activation of NH_3 to $-NH_2$, −NH, and −HNO species on Pt/Al_2O_3-L catalyst was the main reason for its much higher NH_3 oxidation activity. In other words, for Pt catalysts supported on Al_2O_3 support, Pt with relatively lower dispersion and lower oxidation states could better activate NH_3 and thus exhibit higher NH_3 oxidation activity.

4. CONCLUSIONS

Through the simple control of precalcination temperature of bayerite $Al(OH)_3$, the dispersion of Pt species could be fine-tuned from single atoms to small and large clusters on Al_2O_3 support. It was discovered that the concentration of hydroxyl groups on the fresh or precalcined $Al(OH)_3$ supports played a crucial role in determining the dispersion of Pt species. More hydroxyl groups on the fresh or the low-temperature-calcined $Al(OH)_3$ could better facilitate the Pt dispersion via the strong interaction between hydroxyl groups and hydrated Pt ions. In both CO and NH_3 oxidation reactions, Pt/Al_2O_3 catalyst with relatively lower Pt dispersion exhibited much better catalytic performance, mainly due to the higher CO adsorption capacity and more efficient capability in the activation of O_2 and NH_3. This work provides new insights into the precise tuning of Pt dispersion on industrially important Al_2O_3 support using a facile method, and established a clear structure−activity relationship for Pt/Al_2O_3 catalysts in CO and NH_3 oxidation reactions. This study also highlights the significance of not solely pursuing the fabrication of single-atom catalysts but rather prioritizing the achievement of the most efficient Pt species on Al_2O_3 support for specific reactions.

https://doi.org/10.1021/acsami.3c11897
ACS Appl. Mater. Interfaces 2024, 16, 454−466

■ ASSOCIATED CONTENT

Supporting Information

The Supporting Information is available free of charge at https://pubs.acs.org/doi/10.1021/acsami.3c11897.

XAS analysis results, detailed catalyst preparation procedure, XRD, EDS mapping, reaction rates in CO/NH_3 oxidation, N_2 selectivity in NH_3 oxidation reaction, concentrations of byproducts in NH_3 oxidation reaction, CO/NH_3 oxidation activity in long-term test and cyclic test, CO/NH_3 oxidation activity tested in the presence of H_2O, XPS, TG-DTA, in situ DRIFTS of CO-TPR and CO/NH_3 oxidation (PDF)

■ AUTHOR INFORMATION

Corresponding Author

Fudong Liu − *Department of Civil, Environmental, and Construction Engineering, Catalysis Cluster for Renewable Energy and Chemical Transformations (REACT), NanoScience Technology Center (NSTC), University of Central Florida, Orlando, Florida 32816, United States;* orcid.org/0000-0001-8771-5938; Phone: 407-823-6219; Email: fudong.liu@ucf.edu

Authors

Wei Tan − *Department of Civil, Environmental, and Construction Engineering, Catalysis Cluster for Renewable Energy and Chemical Transformations (REACT), NanoScience Technology Center (NSTC), University of Central Florida, Orlando, Florida 32816, United States; State Key Laboratory of Pollution Control and Resource Reuse, School of Environment, Jiangsu Key Laboratory of Vehicle Emissions Control, Center of Modern Analysis, Key Laboratory of Mesoscopic Chemistry of MOE, School of Chemistry and Chemical Engineering, Nanjing University, Nanjing 210023, China;* orcid.org/0000-0002-1481-9346

Shaohua Xie − *Department of Civil, Environmental, and Construction Engineering, Catalysis Cluster for Renewable Energy and Chemical Transformations (REACT), NanoScience Technology Center (NSTC), University of Central Florida, Orlando, Florida 32816, United States;* orcid.org/0000-0003-1550-7421

Xing Zhang − *Department of Civil, Environmental, and Construction Engineering, Catalysis Cluster for Renewable Energy and Chemical Transformations (REACT), NanoScience Technology Center (NSTC), University of Central Florida, Orlando, Florida 32816, United States*

Kailong Ye − *Department of Civil, Environmental, and Construction Engineering, Catalysis Cluster for Renewable Energy and Chemical Transformations (REACT), NanoScience Technology Center (NSTC), University of Central Florida, Orlando, Florida 32816, United States*

Murtadha Almousawi − *Department of Civil, Environmental, and Construction Engineering, Catalysis Cluster for Renewable Energy and Chemical Transformations (REACT), NanoScience Technology Center (NSTC), University of Central Florida, Orlando, Florida 32816, United States*

Daekun Kim − *Department of Civil, Environmental, and Construction Engineering, Catalysis Cluster for Renewable Energy and Chemical Transformations (REACT), NanoScience Technology Center (NSTC), University of Central Florida, Orlando, Florida 32816, United States*

Haowei Yu − *State Key Laboratory of Pollution Control and Resource Reuse, School of Environment, Jiangsu Key Laboratory of Vehicle Emissions Control, Center of Modern Analysis, Key Laboratory of Mesoscopic Chemistry of MOE, School of Chemistry and Chemical Engineering, Nanjing University, Nanjing 210023, China*

Yandi Cai − *State Key Laboratory of Pollution Control and Resource Reuse, School of Environment, Jiangsu Key Laboratory of Vehicle Emissions Control, Center of Modern Analysis, Key Laboratory of Mesoscopic Chemistry of MOE, School of Chemistry and Chemical Engineering, Nanjing University, Nanjing 210023, China*

Hanchen Xi − *State Key Laboratory of Pollution Control and Resource Reuse, School of Environment, Jiangsu Key Laboratory of Vehicle Emissions Control, Center of Modern Analysis, Key Laboratory of Mesoscopic Chemistry of MOE, School of Chemistry and Chemical Engineering, Nanjing University, Nanjing 210023, China*

Lu Ma − *National Synchrotron Light Source II (NSLS-II), Brookhaven National Laboratory, Upton, New York 11973, United States*

Steven N. Ehrlich − *National Synchrotron Light Source II (NSLS-II), Brookhaven National Laboratory, Upton, New York 11973, United States*

Fei Gao − *State Key Laboratory of Pollution Control and Resource Reuse, School of Environment, Jiangsu Key Laboratory of Vehicle Emissions Control, Center of Modern Analysis, Key Laboratory of Mesoscopic Chemistry of MOE, School of Chemistry and Chemical Engineering, Nanjing University, Nanjing 210023, China;* orcid.org/0000-0001-8626-5509

Lin Dong − *State Key Laboratory of Pollution Control and Resource Reuse, School of Environment, Jiangsu Key Laboratory of Vehicle Emissions Control, Center of Modern Analysis, Key Laboratory of Mesoscopic Chemistry of MOE, School of Chemistry and Chemical Engineering, Nanjing University, Nanjing 210023, China;* orcid.org/0000-0002-8393-6669

Complete contact information is available at: https://pubs.acs.org/10.1021/acsami.3c11897

Notes

The authors declare no competing financial interest.

■ ACKNOWLEDGMENTS

F.L. acknowledges the National Science Foundation grant (CHE-1955343) and Startup Fund from the University of Central Florida (UCF). L.D. thanks the support from the National Natural Science Foundation of China (No. 22272077). W.T. thanks the support from the National Natural Science Foundation of China (No. 22306090). S.X., X.Z., and D.K. thank the support from the Preeminent Postdoctoral Program (P3) at UCF. F.L. sincerely thanks Dr. Marcos Schöneborn at Sasol for providing raw materials in catalyst synthesis. This research used beamline 7-BM (QAS) of the National Synchrotron Light Source II, a U.S. Department of Energy (DOE) Office of Science User Facility operated for the DOE Office of Science by Brookhaven National Laboratory under Contract No. DE-SC0012704.

REFERENCES

(1) Reşitoğlu, İ. A.; Altinişik, K.; Keskin, A. The Pollutant Emissions from Diesel-Engine Vehicles and Exhaust Aftertreatment Systems. *Clean Technol. Environ. Policy* **2015**, *17* (1), 15−27.

(2) Twigg, M. V. Progress and Future Challenges in Controlling Automotive Exhaust Gas Emissions. *Appl. Catal., B* **2007**, *70* (1), 2−15.

(3) Wang, A.; Olsson, L. The impact of automotive catalysis on the United Nations sustainable development goals. *Nat. Catal.* **2019**, *2* (7), 566−570.

(4) Datye, A. K.; Votsmeier, M. Opportunities and Challenges in the Development of Advanced Materials for Emission Control Catalysts. *Nat. Mater.* **2021**, *20* (8), 1049−1059.

(5) Xu, H.; Zhang, Z.; Liu, J.; Do-Thanh, C.-L.; Chen, H.; Xu, S.; Lin, Q.; Jiao, Y.; Wang, J.; Wang, Y.; Chen, Y.; Dai, S. Entropy-stabilized single-atom Pd catalysts via high-entropy fluorite oxide supports. *Nat. Commun.* **2020**, *11* (1), No. 3908.

(6) Ivanova, A. S.; Slavinskaya, E. M.; Gulyaev, R. V.; Zaikovskii, V. I.; Stonkus, O. A.; Danilova, I. G.; Plyasova, L. M.; Polukhina, I. A.; Boronin, A. I. Metal-support interactions in Pt/Al_2O_3 and Pd/Al_2O_3 catalysts for CO oxidation. *Appl. Catal., B* **2010**, *97* (1), 57−71.

(7) Boubnov, A.; Dahl, S.; Johnson, E.; Molina, A. P.; Simonsen, S. B.; Cano, F. M.; Helveg, S.; Lemus-Yegres, L. J.; Grunwaldt, J.-D. Structure-activity relationships of Pt/Al_2O_3 catalysts for CO and NO oxidation at diesel exhaust conditions. *Appl. Catal., B* **2012**, *126*, 315−325.

(8) Gänzler, A. M.; Casapu, M.; Doronkin, D. E.; Maurer, F.; Lott, P.; Glatzel, P.; Votsmeier, M.; Deutschmann, O.; Grunwaldt, J.-D. Unravelling the Different Reaction Pathways for Low Temperature CO Oxidation on Pt/CeO_2 and Pt/Al_2O_3 by Spatially Resolved Structure-Activity Correlations. *J. Phys. Chem. Lett.* **2019**, *10* (24), 7698−7705.

(9) Bergman, S. L.; Granestrand, J.; Tang, Y.; París, R. S.; Nilsson, M.; Tao, F. F.; Tang, C.; Pennycook, S. J.; Pettersson, L. J.; Bernasek, S. L. In-situ characterization by Near-Ambient Pressure XPS of the catalytically active phase of Pt/Al_2O_3 during NO and CO oxidation. *Appl. Catal., B* **2018**, *220*, 506−511.

(10) Newton, M. A.; Ferri, D.; Smolentsev, G.; Marchionni, V.; Nachtegaal, M. Kinetic Studies of the Pt Carbonate-Mediated, Room-Temperature Oxidation of Carbon Monoxide by Oxygen over Pt/Al_2O_3 Using Combined, Time-Resolved XAFS, DRIFTS, and Mass Spectrometry. *J. Am. Chem. Soc.* **2016**, *138* (42), 13930−13940.

(11) Allian, A. D.; Takanabe, K.; Fujdala, K. L.; Hao, X.; Truex, T. J.; Cai, J.; Buda, C.; Neurock, M.; Iglesia, E. Chemisorption of CO and Mechanism of CO Oxidation on Supported Platinum Nanoclusters. *J. Am. Chem. Soc.* **2011**, *133* (12), 4498−4517.

(12) Singh, J.; Alayon, E. M. C.; Tromp, M.; Safonova, O. V.; Glatzel, P.; Nachtegaal, M.; Frahm, R.; van Bokhoven, J. A. Generating Highly Active Partially Oxidized Platinum during Oxidation of Carbon Monoxide over Pt/Al_2O_3: In Situ, Time-Resolved, and High-Energy-Resolution X-Ray Absorption Spectroscopy. *Angew. Chem., Int. Ed.* **2008**, *47* (48), 9260−9264.

(13) Chen, Y.; Feng, Y.; Li, L.; Liu, J.; Pan, X.; Liu, W.; Wei, F.; Cui, Y.; Qiao, B.; Sun, X.; Li, X.; Lin, J.; Lin, S.; Wang, X.; Zhang, T. Identification of Active Sites on High-Performance Pt/Al_2O_3 Catalyst for Cryogenic CO Oxidation. *ACS Catal.* **2020**, *10* (15), 8815−8824.

(14) Bus, E.; Ramaker, D. E.; van Bokhoven, J. A. Structure of Ethene Adsorption Sites on Supported Metal Catalysts from in Situ XANES Analysis. *J. Am. Chem. Soc.* **2007**, *129* (26), 8094−8102.

(15) Liu, S.; Xu, H.; Liu, D.; Yu, H.; Zhang, F.; Zhang, P.; Zhang, R.; Liu, W. Identify the Activity Origin of Pt Single-Atom Catalyst via Atom-by-Atom Counting. *J. Am. Chem. Soc.* **2021**, *143* (37), 15243−15249.

(16) Hazlett, M. J.; Epling, W. S. Spatially resolving CO and C_3H_6 oxidation reactions in a Pt/Al_2O_3 model oxidation catalyst. *Catal. Today* **2016**, *267*, 157−166.

(17) Bourane, A.; Derrouiche, S.; Bianchi, D. Impact of Pt dispersion on the elementary steps of CO oxidation by O_2 over Pt/Al_2O_3 catalysts. *J. Catal.* **2004**, *228* (2), 288−297.

(18) Haneda, M.; Watanabe, T.; Kamiuchi, N.; Ozawa, M. Effect of platinum dispersion on the catalytic activity of Pt/Al_2O_3 for the oxidation of carbon monoxide and propene. *Appl. Catal., B* **2013**, *142−143*, 8−14.

(19) Slavinskaya, E. M.; Kibis, L. S.; Stonkus, O. A.; Svintsitskiy, D. A.; Stadnichenko, A. I.; Fedorova, E. A.; Romanenko, A. V.; Marchuk, V.; Doronkin, D. E.; Boronin, A. I. The Effects of Platinum Dispersion and Pt State on Catalytic Properties of Pt/Al_2O_3 in NH_3 Oxidation. *ChemCatChem* **2021**, *13* (1), 313−327.

(20) Kwak, J. H.; Hu, J.; Mei, D.; Yi, C.-W.; Kim, D. H.; Peden, C. H. F.; Allard, L. F.; Szanyi, J. Coordinatively Unsaturated Al^{3+} Centers as Binding Sites for Active Catalyst Phases of Platinum on γ-Al_2O_3. *Science* **2009**, *325* (5948), 1670−1673.

(21) Zhang, Z.; Zhu, Y.; Asakura, H.; Zhang, B.; Zhang, J.; Zhou, M.; Han, Y.; Tanaka, T.; Wang, A.; Zhang, T.; Yan, N. Thermally stable single atom Pt/m-Al_2O_3 for selective hydrogenation and CO oxidation. *Nat. Commun.* **2017**, *8* (1), No. 16100.

(22) Chen, Y.; Lin, J.; Jia, B.; Wang, X.; Jiang, S.; Ma, T. Isolating Single and Few Atoms for Enhanced Catalysis. *Adv. Mater.* **2022**, *34* (39), No. 2201796.

(23) Tomboc, G. M.; Kim, T.; Jung, S.; Yoon, H. J.; Lee, K. Modulating the Local Coordination Environment of Single-Atom Catalysts for Enhanced Catalytic Performance in Hydrogen/Oxygen Evolution Reaction. *Small* **2022**, *18* (17), No. 2105680.

(24) Wang, T.; Jia, L.-W.; Wang, X.-T.; Wang, G.; Luo, F.-Q.; Wang, J.-M. Enhancing low-temperature NO_x storage and reduction performance of a Pt-based lean NO_x trap catalyst. *Rare Met.* **2019**, *38* (1), 81−86.

(25) Xie, S.; Zhang, X.; Xu, P.; Hatcher, B.; Liu, Y.; Ma, L.; Ehrlich, S. N.; Hong, S.; Liu, F. Effect of surface acidity modulation on Pt/Al_2O_3 single atom catalyst for carbon monoxide oxidation and methanol decomposition. *Catal. Today* **2022**, *402*, 149−160.

(26) Yan, Z.; Yang, H.; Ouyang, J.; Tang, A. In situ loading of highly-dispersed CuO nanoparticles on hydroxyl-group-rich SiO_2-AlOOH composite nanosheets for CO catalytic oxidation. *Chem. Eng. J.* **2017**, *316*, 1035−1046.

(27) Wang, F.; Ma, J.; Xin, S.; Wang, Q.; Xu, J.; Zhang, C.; He, H.; Cheng Zeng, X. Resolving the puzzle of single-atom silver dispersion on nanosized γ-Al_2O_3 surface for high catalytic performance. *Nat. Commun.* **2020**, *11* (1), No. 529.

(28) Zhang, Z.; He, G.; Li, Y.; Zhang, C.; Ma, J.; He, H. Effect of Hydroxyl Groups on Metal Anchoring and Formaldehyde Oxidation Performance of Pt/Al_2O_3. *Environ. Sci. Technol.* **2022**, *56* (15), 10916−10924.

(29) Zhao, Y.; Chen, D.; Liu, J.; He, D.; Cao, X.; Han, C.; Lu, J.; Luo, Y. Tuning the metal-support interaction on chromium-based catalysts for catalytically eliminate methyl mercaptan: Anchored active chromium species through surface hydroxyl groups. *Chem. Eng. J.* **2020**, *389*, No. 124384.

(30) Farajimotlagh, M.; Poursalehi, R.; Aliofkhazraei, M. Synthesis mechanisms, optical and structural properties of η-Al_2O_3 based nanoparticles prepared by DC arc discharge in environmentally friendly liquids. *Ceram. Int.* **2017**, *43* (10), 7717−7723.

(31) Seo, C. W.; Jung, K. D.; Lee, K. Y.; Yoo, K. S. Influence of Structure Type of Al_2O_3 on Dehydration of Methanol for Dimethyl Ether Synthesis. *Ind. Eng. Chem. Res.* **2008**, *47* (17), 6573−6578.

(32) Sun, R.; Shen, S.; Zhang, D.; Ren, Y.; Fan, J. Hydrofining of Coal Tar Light Oil to Produce High Octane Gasoline Blending Components over γ-Al_2O_3- and η-Al_2O_3-Supported Catalysts. *Energy Fuels* **2015**, *29* (11), 7005−7013.

(33) Wang, Y.; Kou, L.; Lu, J.; Han, D.; Zhang, Z.; Sun, H.; Dai, C.; Mao, Y.; Yan, Z. One-step synthesis of egg-tray-like layered ordered macro-mesoporous SiO_2-Al_2O_3 composites for enhanced hydrodesulfurization performance. *Microporous Mesoporous Mater.* **2021**, *322*, No. 111131.

(34) Moses-DeBusk, M.; Yoon, M.; Allard, L. F.; Mullins, D. R.; Wu, Z.; Yang, X.; Veith, G.; Stocks, G. M.; Narula, C. K. CO Oxidation on Supported Single Pt Atoms: Experimental and ab Initio Density

https://doi.org/10.1021/acsami.3c11897
ACS Appl. Mater. Interfaces 2024, 16, 454−466

Functional Studies of CO Interaction with Pt Atom on θ-Al_2O_3(010) Surface. *J. Am. Chem. Soc.* **2013**, *135* (34), 12634−12645.
(35) Zhao, S.; Lin, J.; Wu, P.; Ye, C.; Li, Y.; Li, A.; Jin, X.; Zhao, Y.; Chen, G.; Qiu, Y.; Ye, D. A Hydrothermally Stable Single-Atom Catalyst of Pt Supported on High-Entropy Oxide/Al_2O_3: Structural Optimization and Enhanced Catalytic Activity. *ACS Appl. Mater. Interfaces* **2021**, *13* (41), 48764−48773.
(36) Sun, G.; Zhao, Z.-J.; Mu, R.; Zha, S.; Li, L.; Chen, S.; Zang, K.; Luo, J.; Li, Z.; Purdy, S. C.; Kropf, A. J.; Miller, J. T.; Zeng, L.; Gong, J. Breaking the scaling relationship via thermally stable Pt/Cu single atom alloys for catalytic dehydrogenation. *Nat. Commun.* **2018**, *9* (1), No. 4454.
(37) Ding, K.; Gulec, A.; Johnson, A. M.; Schweitzer, N. M.; Stucky, G. D.; Marks, L. D.; Stair, P. C. Identification of Active Sites in CO Oxidation and Water-Gas Shift over Supported Pt Catalysts. *Science* **2015**, *350* (6257), 189−192.
(38) Avanesian, T.; Dai, S.; Kale, M. J.; Graham, G. W.; Pan, X.; Christopher, P. Quantitative and Atomic-Scale View of CO-Induced Pt Nanoparticle Surface Reconstruction at Saturation Coverage via DFT Calculations Coupled with *in Situ* TEM and IR. *J. Am. Chem. Soc.* **2017**, *139* (12), 4551−4558.
(39) Wang, C.; Gu, X.-K.; Yan, H.; Lin, Y.; Li, J.; Liu, D.; Li, W.-X.; Lu, J. Water-Mediated Mars-Van Krevelen Mechanism for CO Oxidation on Ceria-Supported Single-Atom Pt_1 Catalyst. *ACS Catal.* **2017**, *7* (1), 887−891.
(40) Zhao, S.; Chen, F.; Duan, S.; Shao, B.; Li, T.; Tang, H.; Lin, Q.; Zhang, J.; Li, L.; Huang, J.; Bion, N.; Liu, W.; Sun, H.; Wang, A.-Q.; Haruta, M.; Qiao, B.; Li, J.; Liu, J.; Zhang, T. Remarkable active-site dependent H_2O promoting effect in CO oxidation. *Nat. Commun.* **2019**, *10* (1), No. 3824.
(41) Tan, W.; Xie, S.; Le, D.; Diao, W.; Wang, M.; Low, K.-B.; Austin, D.; Hong, S.; Gao, F.; Dong, L.; Ma, L.; Ehrlich, S. N.; Rahman, T. S.; Liu, F. Fine-tuned local coordination environment of Pt single atoms on ceria controls catalytic reactivity. *Nat. Commun.* **2022**, *13* (1), No. 7070.
(42) Tan, W.; Cai, Y.; Yu, H.; Xie, S.; Wang, M.; Ye, K.; Ma, L.; Ehrlich, S. N.; Gao, F.; Dong, L.; Liu, F. Tuning the Interaction between Platinum Single Atoms and Ceria by Zirconia Doping for Efficient Catalytic Ammonia Oxidation. *Environ. Sci. Technol.* **2023**, *57* (41), 15747−15758.
(43) Koichumanova, K.; Sai Sankar Gupta, K. B.; Lefferts, L.; Mojet, B. L.; Seshan, K. An in situ ATR-IR spectroscopy study of aluminas under aqueous phase reforming conditions. *Phys. Chem. Chem. Phys.* **2015**, *17* (37), 23795−23804.
(44) Al-Abadleh, H. A.; Grassian, V. H. FT-IR Study of Water Adsorption on Aluminum Oxide Surfaces. *Langmuir* **2003**, *19* (2), 341−347.
(45) Vasilchenko, D.; Tkachenko, P.; Tkachev, S.; Popovetskiy, P.; Komarov, V.; Asanova, T.; Asanov, I.; Filatov, E.; Maximovskiy, E.; Gerasimov, E.; Zhurenok, A.; Kozlova, E. Sulfuric Acid Solutions of $[Pt(OH)_4(H_2O)_2]$: A Platinum Speciation Survey and Hydrated Pt(IV) Oxide Formation for Practical Use. *Inorg. Chem.* **2022**, *61* (25), 9667−9684.
(46) Lee, J.; Jang, E. J.; Oh, D. G.; Szanyi, J.; Kwak, J. H. Morphology and size of Pt on Al_2O_3: The role of specific metal-support interactions between Pt and Al_2O_3. *J. Catal.* **2020**, *385*, 204−212.
(47) Tan, W.; Wang, J.; Li, L.; Liu, A.; Song, G.; Guo, K.; Luo, Y.; Liu, F.; Gao, F.; Dong, L. Gas Phase Sulfation of Ceria-Zirconia Solid Solutions for Generating Highly Efficient and SO_2 Resistant NH_3-SCR Catalysts for NO Removal. *J. Hazard. Mater.* **2020**, *388*, No. 121729.
(48) Xu, G.; Ma, J.; Wang, L.; Lv, Z.; Wang, S.; Yu, Y.; He, H. Mechanism of the H_2 Effect on NH_3-Selective Catalytic Reduction over Ag/Al_2O_3: Kinetic and Diffuse Reflectance Infrared Fourier Transform Spectroscopy Studies. *ACS Catal.* **2019**, *9* (11), 10489−10498.
(49) Sun, M.; Liu, J.; Song, C.; Ogata, Y.; Rao, H.; Zhao, X.; Xu, H.; Chen, Y. Different Reaction Mechanisms of Ammonia Oxidation Reaction on Pt/Al_2O_3 and Pt/$CeZrO_2$ with Various Pt States. *ACS Appl. Mater. Interfaces* **2019**, *11* (26), 23102−23111.
(50) Tan, W.; Liu, A.; Xie, S.; Yan, Y.; Shaw, T. E.; Pu, Y.; Guo, K.; Li, L.; Yu, S.; Gao, F.; Liu, F.; Dong, L. Ce-Si Mixed Oxide: A High Sulfur Resistant Catalyst in the NH_3-SCR Reaction through the Mechanism-Enhanced Process. *Environ. Sci. Technol.* **2021**, *55* (6), 4017−4026.
(51) Wang, F.; Ma, J.; He, G.; Chen, M.; Zhang, C.; He, H. Nanosize Effect of Al_2O_3 in Ag/Al_2O_3 Catalyst for the Selective Catalytic Oxidation of Ammonia. *ACS Catal.* **2018**, *8* (4), 2670−2682.
(52) Wang, F.; He, G.; Zhang, B.; Chen, M.; Chen, X.; Zhang, C.; He, H. Insights into the Activation Effect of H_2 Pretreatment on Ag/Al_2O_3 Catalyst for the Selective Oxidation of Ammonia. *ACS Catal.* **2019**, *9* (2), 1437−1445.
(53) Amores, J. G.; Escribano, V. S.; Ramis, G.; Busca, G. An FT-IR study of ammonia adsorption and oxidation over anatase-supported metal oxides. *Appl. Catal., B* **1997**, *13* (1), 45−58.
(54) Chen, W.; Qu, Z.; Huang, W.; Hu, X.; Yan, N. Novel effect of SO_2 on selective catalytic oxidation of slip ammonia from coal-fired flue gas over IrO_2 modified Ce−Zr solid solution and the mechanism investigation. *Fuel* **2016**, *166*, 179−187.
(55) Kantcheva, M. Identification, Stability, and Reactivity of NO_x Species Adsorbed on Titania-Supported Manganese Catalysts. *J. Catal.* **2001**, *204* (2), 479−494.
(56) Zhang, Q.; Zhang, T.; Xia, F.; Zhang, Y.; Wang, H.; Ning, P. Promoting effects of acid enhancing on N_2 selectivity for selectivity catalytic oxidation of NH_3 over RuO_x/TiO_2: The mechanism study. *Appl. Surf. Sci.* **2020**, *500*, No. 144044.
(57) Chen, W.; Ma, Y.; Qu, Z.; Liu, Q.; Huang, W.; Hu, X.; Yan, N. Mechanism of the Selective Catalytic Oxidation of Slip Ammonia over Ru-Modified Ce−Zr Complexes Determined by in Situ Diffuse Reflectance Infrared Fourier Transform Spectroscopy. *Environ. Sci. Technol.* **2014**, *48* (20), 12199−12205.
(58) Chen, J. P.; Hausladen, M. C.; Yang, R. T. Delaminated Fe_2O_3-Pillared Clay: Its Preparation, Characterization, and Activities for Selective Catalytic Reduction of No by NH_3. *J. Catal.* **1995**, *151* (1), 135−146.

https://doi.org/10.1021/acsami.3c11897
ACS Appl. Mater. Interfaces 2024, 16, 454−466